Volume 48
Number 14
14 April 2024
Pages 6043–6516

NJC

New Journal of Chemistry

A journal for new directions in chemistry

rsc.li/njc

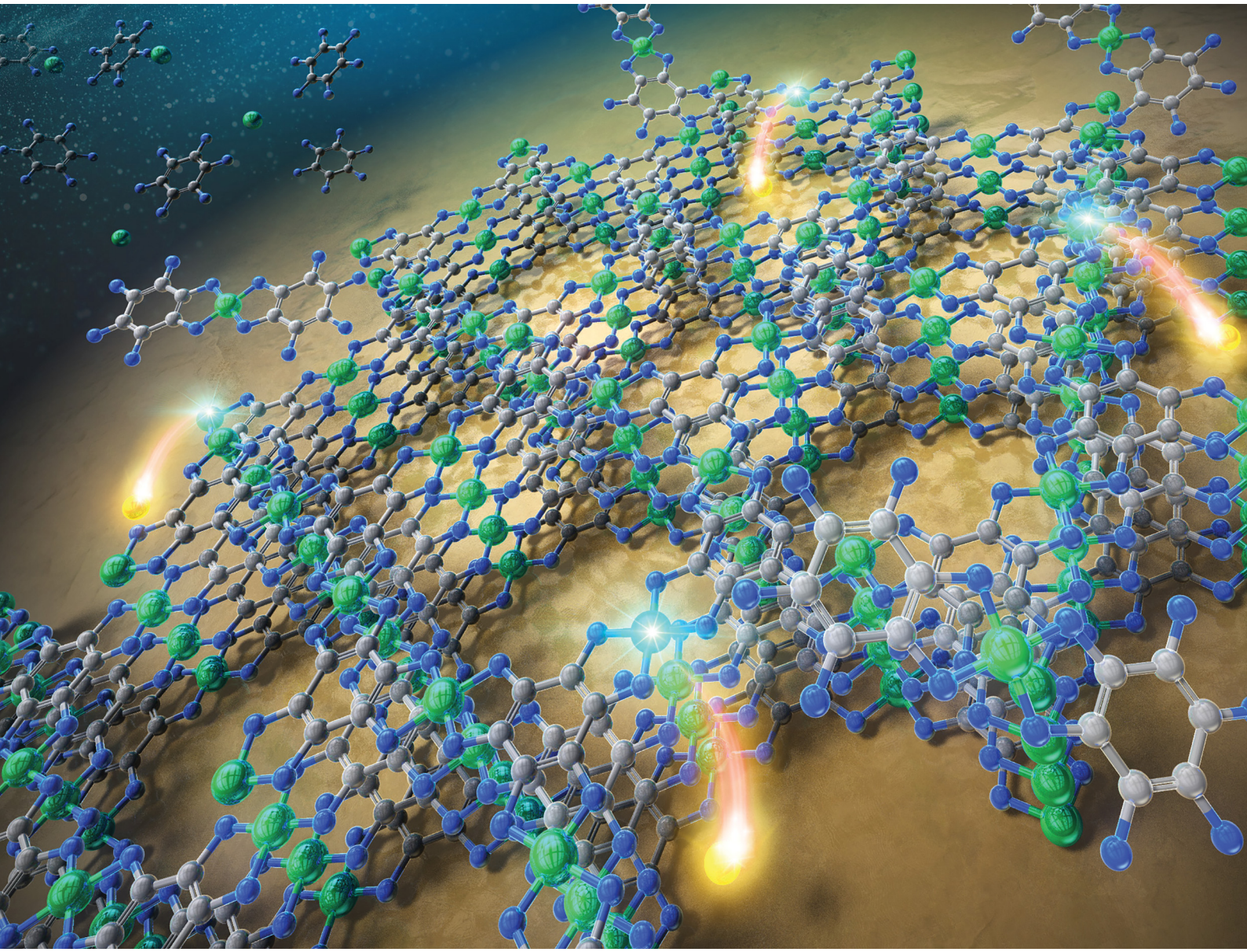

ISSN 1144-0546

ROYAL SOCIETY OF CHEMISTRY

PAPER

Hiroaki Maeda, Hiroshi Nishihara *et al.*
Face-on-oriented formation of bis(diimino)metal coordination nanosheets on gold electrodes by electrochemical oxidation

cnrs

NJC

ROYAL SOCIETY OF CHEMISTRY

PAPER

View Article Online
View Journal | View Issue

Cite this: *New J. Chem.*, 2024, **48**, 6081

Face-on-oriented formation of bis(diimino)metal coordination nanosheets on gold electrodes by electrochemical oxidation†

Hiroaki Maeda, *[a] Kenji Takada, [a] Naoya Fukui,[a] Hiroyasu Masunaga,[b] Sono Sasaki,[cd] Kazuhito Tsukagoshi [e] and Hiroshi Nishihara*[af]

Bis(diimino)metal complex nanosheets composed of metal ions and hexaaminobenzene ligands (MHABs) are fascinating two-dimensional materials which have been gaining significant attention as electrode materials and electrocatalysts owing to their electrical conductivities, redox properties, and porous structures obtained by the π-conjugated system and regular metal complex arrangement. Although electrochemical oxidation enables the simple and direct formation of MHABs on electrodes within a couple of minutes only, the obtained MHABs are relatively rough and of low crystallinity. This study investigated the effects of the applied potential during the synthesis, the type of base, and the concentrations of bases and building blocks on the synthesis of NiHAB nanosheets. Optical microscopy (OM), atomic force microscopy (AFM), Raman spectroscopy, X-ray photoelectron spectroscopy (XPS), and grazing-incidence X-ray scattering (GIXS) results revealed that a low oxidation potential, high concentration of the ammonia solution, and low concentration of the building blocks in the reaction solution provided a nanometre-thick NiHAB layer. Under the optimal reaction conditions, NiHAB nanosheets were successfully synthesized in a face-on orientation manner on gold electrodes using electrochemical oxidation methods. Furthermore, the anisotropic electrochemical synthesis of CuHAB was achieved under the optimised conditions. The mechanism of the MHAB growth process with an anisotropic orientation and nanometre thickness was proposed and attributed to the flat adsorption of π-conjugated oligomers composed of bis(diamino)metal moieties in a solution onto an electrode surface and the electrochemical oxidation and deprotonation of the adsorbates on the electrode.

Received 8th December 2023,
Accepted 28th February 2024

DOI: 10.1039/d3nj05650c

rsc.li/njc

Introduction

Organic two-dimensional materials have been recently gaining significant attention owing to their designable and tailorable chemical structure.[1–3] In particular, electrically conductive coordination nanosheets (CONASHs),[4,5] also known as conductive metal–organic frameworks,[6–10] have been employed in various applications such as electronics, energy storage devices, sensing devices, and electrocatalysts owing to their fascinating electrical conductivities derived from their π-conjugated structures, redox activities, large surface areas, and porous structures. Since the synthesis of crystalline CONASH production is essential for unveiling their inherent conductive properties and enhancing their performance by minimising the effect of amorphous phases, boundaries, and defects, studies have focused on the synthesis of highly crystalline or single-crystalline samples. Several studies have reported the successful synthesis of highly crystalline CONASHs and their conductive properties were also investigated.[11–14]

Metal-hexaaminobenzene (MHAB) nanosheets are attractive conductive CONASHs that can be employed as cathode

[a] *Research Institute for Science and Technology, Tokyo University of Science, 2641 Yamazaki, Noda, Chiba, 278-8510, Japan. E-mail: h-maeda@rs.tus.ac.jp, nisihara@rs.tus.ac.jp*
[b] *Japan Synchrotron Radiation Research Institute (JASRI), 1-1-1 Kouto, Sayo-cho, Sayo-gun, Hyogo 679-5198, Japan*
[c] *Faculty of Fibre Science and Engineering, Kyoto Institute of Technology, Matsugasaki, Sakyo-ku, Kyoto 606-8585, Japan*
[d] *RIKEN SPring-8 Centre, 1-1-1 Kouto, Sayo-cho, Sayo-gun, Hyogo, 679-5148, Japan*
[e] *Research Centre for Materials Nanoarchitectonics (MANA), National Institute for Materials Science (NIMS), 1-1 Namiki, Tsukuba, Ibaraki 305-0044, Japan*
[f] *Graduate School of Science and Technology, Tokyo University of Science, 2641 Yamazaki, Noda, Chiba, 278-8510, Japan*

† Electronic supplementary information (ESI) available: Experimental details; GIXS of bare Au/glass substrate; photographs of prepared electrodes; CV of electrolyte solution for NiHAB synthesis; Raman and XP spectra of NiHAB-A and NiHAB-B; CV of NiHAB-B; CVs of electrolyte solutions for NiHAB-C, NiHAB-D, and NiHAB-E synthesis; optical microscope images and Raman and XP spectra of NiHAB-C, NiHAB-D, and NiHAB-E; Roughness analyses, Raman, and XP spectra of NiHAB-F and NiHAB-G; two-dimensional scattering image and diffraction pattern of NiHAB-F. CV of electrolyte solution for CoHAB synthesis; Raman spectra and two-dimensional scattering patterns of CoHAB-A and CoHAB-B; cyclic voltammogram of electrolyte solution for CuHAB synthesis; characterization of CuHAB-B and CuHAB-F; CVs of CoHAB-B and CuHAB-F. See DOI: **https://doi.org/10.1039/d3nj05650c**

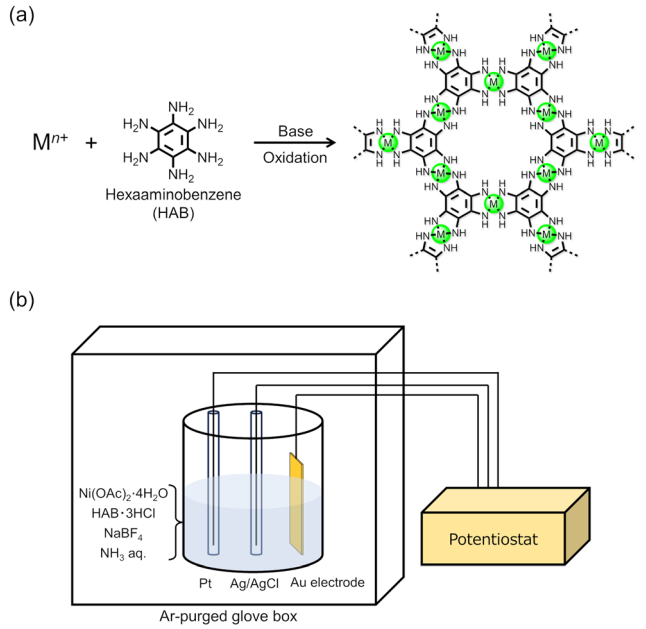

Fig. 1 (a) Schematic representation of the synthesis of MHAB CONASHs. (b) Schematic illustration of the electrochemical synthesis of NiHAB on gold electrodes.

materials in secondary ion batteries,[15–17] electrode materials for supercapacitors,[18–20] and chemiresistive sensors.[21,22] They can be also employed as electrocatalysts for the hydrogen evolution reaction (HER)[23] and for the oxygen evolution[24] and oxygen reduction reactions.[25] Furthermore, they can be quickly and easily synthesised by the electrochemical oxidation processes[23,26] (Fig. 1). Our group has previously reported the synthesis of MHABs (M = Co, Ni, Cu) by using an electrochemical oxidation method by applying an oxidation potential for 10–180 s on a working electrode in an electrolyte solution of a metal ion and HAB.[23,26]

The ability to directly employ the MHAB-modified electrodes as electrocatalysts for a HER was also investigated. Nevertheless, the MHABs formed on the electrodes were rough and low crystalline since controlling the uniformity of the film was difficult under these conditions. It should be noted that we succeeded in controlling the crystallinity of HAB-based CONASHs for copper by manipulating the reaction conditions of the liquid–liquid interfacial synthesis.[27]

This study investigated the optimum reaction conditions (applied oxidation potential and concentrations of the chemical reagents) for the synthesis of crystalline NiHABs on gold electrodes by using an electrochemical oxidation method. Optical microscopy (OM), atomic force microscopy (AFM), Raman spectroscopy, X-ray photoelectron spectroscopy (XPS), and 2D grading-incidence X-ray scattering (GIXS) revealed the anisotropic formation of NiHABs in a face-on orientation manner on the electrodes. Furthermore, the anisotropic synthesis of CuHAB on a gold electrode was also assessed under the optimised conditions. Finally, a possible mechanism of the MHAB growth process using the electrochemical oxidation method was also proposed.

Results and discussion

Oxygen in air works as an oxidizing agent and advances MHAB formation before the oxidation potential is applied. To prevent this oxygen-assisted NiHAB formation in air, the electrochemical synthesis of NiHABs on a gold electrode was carried out in an Ar-purged glovebox with solvents degassed with nitrogen. Ag/AgCl, Pt, and Au/glass employed as the reference, counter, and working electrodes, respectively, were immersed in an aqueous ammonia (conc. NH_3 aq./H_2O = 1 : 5, *ca.* 2.3 M) solution in the presence of $NaBF_4$, $Ni(OAc)_2$, and HAB·3HCl (Fig. 1b). Initially, we investigated the optimum applied potential during NiHAB formation since our group has recently reported that the crystallinity of CuHAB synthesised at a liquid–liquid interface in the presence of a weak oxidising agent was enhanced.[27] It was thus hypothesised that applying a low oxidation potential could induce the formation of more crystalline NiHABs. To investigate the effect of applied oxidation potential precisely, we employed the chronoamperometry technique to only apply the targeted potential to the working electrode instead of the cyclic voltammetry technique which has been often used in electrochemical polymerization.[28–30] Although an oxidation potential of +0.56 ∼ +0.58 V *vs.* Ag/AgCl was applied to the working electrode in previous studies,[23,26] we hypothesised

Table 1 Synthetic conditions for MHAB-X (M = Ni, Co, Cu, X = A–G) electrochemical synthesis

Condition	Applied potential (V *vs.* Ag/AgCl)	Base	Base concentration (mol L^{-1})	Metal ion concentration (μmol in 5 mL)	HAB concentration (μmol in 5 mL)
A	High NiHAB: +0.58 CoHAB: +0.21	NH_3	2.3	6	4
B	Low NiHAB: −0.10 CoHAB: −0.10 CuHAB: −0.20	NH_3	2.3	6	4
C	Low	NH_3	0.1	6	4
D	Low	TEA[a]	0.1	6	4
E	Low	EDA[b]	0.1	6	4
F	Low	NH_3	2.3	0.6	0.4
G	Low	NH_3	0.1	0.6	0.4

[a] Triethylamine. [b] Ethylenediamine.

that a potential of −0.10 V *vs.* Ag/AgCl, which corresponds to the potential at the end of the first oxidation peak at −0.27 V *vs.* Ag/AgCl, is enough to advance the oxidation process in the NiHAB formation (Fig. S2, ESI†). NiHAB-A and NiHAB-B were prepared by applying oxidation potentials at +0.58 V and −0.10 V *vs.* Ag/AgCl for 180 s, respectively (Table 1 see also the ESI† for further experimental details). In the case of NiHAB-B, the colour of the lower area (*ca.* 20 mm × 5 mm) of the Au electrode changed due to the NiHAB formation while NiHAB-A did not show an obvious colour change (Fig. S3, ESI†). The OM images of NiHAB-A and NiHAB-B revealed clear differences between the two modified surfaces (Fig. 2a and b), where black domains were sparsely present on the NiHAB-A surface, while the NiHAB-B surface was covered with a grey film and exhibited smaller black domains. The high-resolution AFM images at the boundary of the unmodified and NiHAB-modified surfaces revealed topographical differences (Fig. 2c and d). NiHAB-A showed many spherical structures expected to be NiHAB domains with heights of approximately 25 nm, while NiHAB-B showed a uniformly modified area with a thickness of ∼6 nm, corresponding to ∼20 layers of NiHAB. These results confirmed the suitability of a low oxidation potential for the uniform formation of NiHAB on an electrode. The Raman spectra collected at the black domains on NiHAB-A and the grey film area on NiHAB-B exhibited peaks at 440, 615, and 1510 cm^{-1} which are in accordance with the reported spectra of NiHAB, thus indicating the formation of NiHAB at both oxidation potentials (Fig. S4a, ESI†).[16] However, the Raman spectra of the areas between the black domains did not show any significant peaks, thus indicating the absence of NiHAB and exposure of the gold surface (Fig. S4b, ESI†). The results show that electrochemical oxidation at a high oxidation potential caused the spot formation of NiHAB on the electrode surface, thus inducing a rough surface morphology, which is in accordance with the results of a previous study.[26] XPS revealed peaks at 854.7, 872.3, and 397.8 eV attributed to those of Ni $2p_{3/2}$, Ni $2p_{1/2}$, and N 1s, respectively, which were in accordance with previously reported values suggesting that the nickel centre is divalent (Fig. S5, ESI†).[23,26] The calculated Ni : N atomic ratios of NiHAB-A and NiHAB-B were 1 : 4.9 and 1 : 5.4, respectively. These values suggest the presence of slightly excess nitrogen atoms compared with the ideal atomic ratio for the bis(diamino)nickel complex, Ni : N = 1 : 4. The absence of Na, Cl, and F, the components of HAB·3HCl and $NaBF_4$, indicated that NiHAB-A and NiHAB-B were in the neutral (zero-valence) states, and that these elements were present neither in the cationic nor in the anionic form (Fig. S5, ESI†).

The crystallinities of NiHAB-A and NiHAB-B were evaluated by GIXS (Fig. 3a and b). The two-dimensional scattering image and XRD patterns obtained by integrating the scattering pattern of NiHAB-A did not exhibit any significant signal which can be attributed either to its amorphous nature or very low crystallinity (Fig. 3a). NiHAB-B produced two spots in the in-plane direction and one spot in the out-of-plane direction in the scattering image which can be attributed to the XRD peaks at 5° and 17.5°, respectively (Fig. 3b). Upon their comparison with the simulated XRD pattern of NiHAB in the eclipsed (AA) stacking structure with the unit cell parameters *P*6/*mmm*, a = 13.01 Å and c = 3.25 Å, these peaks were attributed to the diffraction from the (1 0 0) and (0 0 1) planes of NiHAB, respectively (Fig. 3c).[26] Furthermore, the two-dimensional scattering image reflected the crystal anisotropy of NiHAB-B. The XRD pattern of NiHAB-B extracted from the in-plane

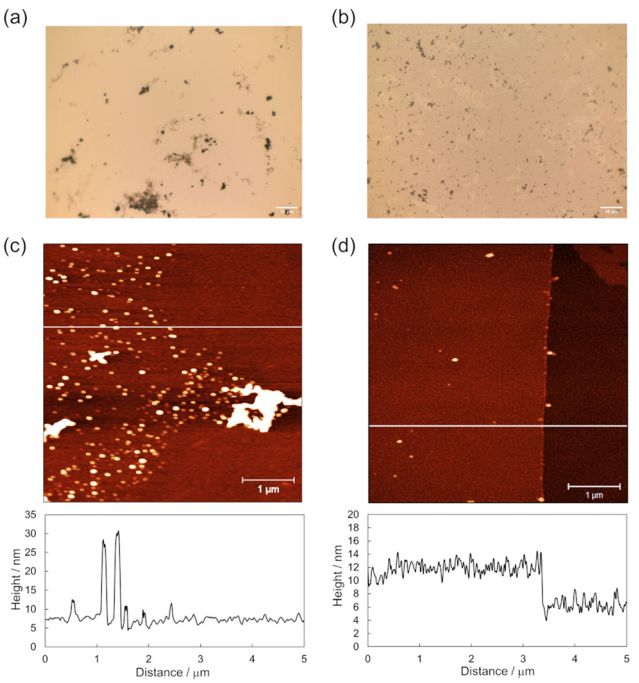

Fig. 2 OM images of (a) NiHAB-A and (b) NiHAB-B, and AFM topography images and height profiles at the corresponding white lines of (c) NiHAB-A and (d) NiHAB-B.

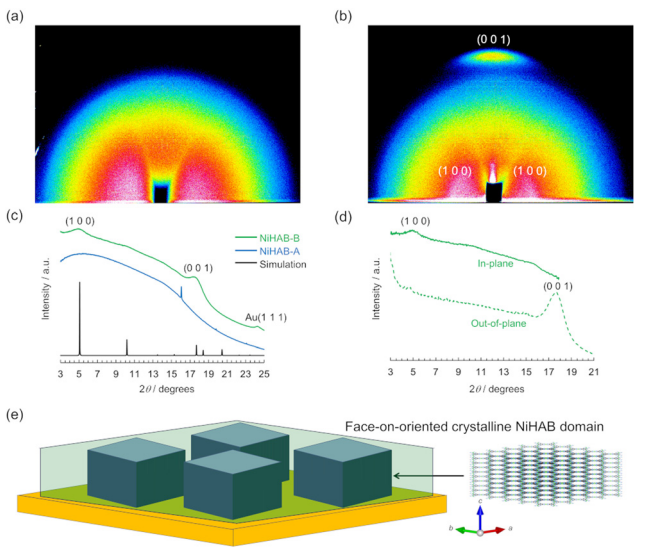

Fig. 3 Two-dimensional scattering images obtained by GIXS measurements of (a) NiHAB-A and (b) NiHAB-B. (c) Diffraction patterns converted from the scattering images. (d) In-plane (solid line) and out-of-plane (dashed line) diffraction profiles of NiHAB-B. (e) Schematic representation of NiHAB in a face-on orientation manner formed on an Au electrode. Gray blocks represent face-on-oriented crystalline NiHAB domains and the green part represents NiHAB films formed on the electrode.

direction of the scattering image showed only one peak corresponding to the (1 0 0) plane, while only the peak of the (0 0 1) plane was observed in the out-of-plane direction, suggesting an anisotropic NiHAB formation in a face-on fashion on a gold surface at the oxidation potential of −0.10 V *vs.* Ag/AgCl (Fig. 3d and e). These results revealed that electrochemical oxidation at the low potential allows an anisotropic formation of NiHAB with a thickness of several nanometres. To the best of our knowledge, this is the first success of the direct orientation observation of electrochemically synthesized HAB-based CONASHs on electrodes. The type of base and concentrations of the base, nickel ion, and HAB were then optimised to obtain more uniform and thinner NiHABs using the electrochemical oxidation method.

The electrochemical activity of NiHAB-B was also investigated in a 1 M $^{n}Bu_4NPF_6/CH_3CN$ electrolyte solution (Fig. S6, ESI†). A redox couple of around 0.2 V *vs.* ferrocenium/ferrocene (Fc^+/Fc) derives from the redox reaction of bis(diimino)nickel units in NiHAB. A similar redox behaviour was also observed in NiHABs synthesized by the gas–liquid interfacial synthesis and the electrochemical oxidation method at the high oxidation potential.[26]

To investigate the effect of the base type and concentration on NiHAB formation, the NiHABs were synthesised with aqueous solutions of three different bases: NH_3 (0.1 M), triethylamine (0.1 M, TEA), ethylenediamine (0.1 M, EDA) instead of the 2.3 M NH_3 solution (Table 1). The cyclic voltammograms of these reaction mixtures were measured to confirm the suitability of the oxidation at −0.10 V for the synthesis of NiHAB under these conditions (Fig. S7, ESI†). The appearance of the first oxidation peak at −0.265 V *vs.* Ag/AgCl in the NH_3 solution (0.1 M) and two oxidation peaks at approximately −0.28 V and −0.18 V *vs.* Ag/AgCl in the TEA and EDA solutions, respectively, indicated that an oxidation potential of −0.10 V can sufficiently promote the oxidation reaction for NiHAB formation. Hence, the electrochemical formation of NiHAB in the NH_3 (0.1 M), TEA, and EDA solutions at −0.10 V for 180 s to prepare NiHAB-C, NiHAB-D, and NiHAB-E, respectively (Fig. S3, ESI†). NiHAB-C exhibited a brown-coloured modified area of approximately 20 mm × 5 mm while NiHAB-D and NiHAB-E did not show obvious colour changes in the electrode surfaces. The OM images revealed that the NiHAB-C surface was covered with a grey film and small black domains, similar to the NiHAB-B prepared under the higher base concentration conditions (Fig. S8a, ESI†). NiHAB-D exhibited black film domains with a lateral size >10 μm, and NiHAB-E showed small film domains with a lateral size of a few micrometres. The presence of the reported peaks in the microscopic Raman spectra measurements revealed NiHAB formation on NiHAB-C (Fig. S8b, ESI†). The black domains in NiHAB-D were characterised as NiHAB whereas the gold surface was exposed without film formation in the remaining area (Fig. S8c, ESI†). The film observed on NiHAB-E showed a peak at approximately 2860 cm^{-1} attributed to the C–H stretching vibration, thus implying the formation of an organic compound including EDA instead of NiHAB, while other significant peaks were not observed in the remaining area (Fig. S8d, ESI†). It was thus concluded that TEA and EDA are unsuitable for the electrochemically assisted synthesis of NiHAB because of their strong coordination abilities with metal ions which compete for HAB, and thus prevent the complexation between nickel ions and HAB.[31] XP spectra of NiHAB-C showed Ni $2p_{3/2}$, Ni $2p_{1/2}$, and N 1s peaks at 855.2 eV, 872.2 eV, and 398.2 eV, respectively, with the Ni:N atomic ratio of 1 : 5.8, suggesting the formation of NiHAB with the slightly excess amount of nitrogen (Fig. S9a, ESI†). On the other hand, NiHAB-D and NiHAB-E gave weak peaks derived from Ni 2p and N 1s in the XP spectra (Fig. S9b and c, ESI†). In addition, the respective Ni : N atomic ratios calculated to be 1 : 32 and 1 : 13 were far from identical values. The Raman and XP spectra results indicate the NiHAB formation in NiHAB-C and the insufficient nanosheet formation in NiHAB-D and NiHAB-E. Hence, we conducted further topography and crystallinity evaluations only for NiHAB-C.

The AFM images at the boundary of the modified area and bare gold exhibited a film with a thickness of 10 nm in addition to the presence of spherical particles with heights exceeding 10 nm on the film (Fig. 4a). These particles were estimated to have overreacted with the NiHAB grown on the NiHAB film. The appearance of in-plane scattering spots for the (1 0 0) and (2 0 0) planes and an out-of-plane scattering spot of the (0 0 1) plane in the 2D GIXS scattering image in addition to the XRD diffraction peaks at 5°, 10°, and 17.5° confirmed the face-on anisotropic formation of crystalline NiHAB on the electrode (Fig. 4b and c).

Although the optimisation of the reaction conditions described above revealed that the application of a low oxidation potential in NH_3 aq. with an electrolyte is suitable for the anisotropic growth of NiHABs on an electrode, black domains, considered as spotty-grown NiHABs, were still present on NiHAB-B and NiHAB-C. To prevent overgrowth after film formation, the electrochemical synthesis was performed by diluting the nickel ion and HAB ligand concentrations ten times. NiHAB-F and NiHAB-G were thus prepared using ammonia

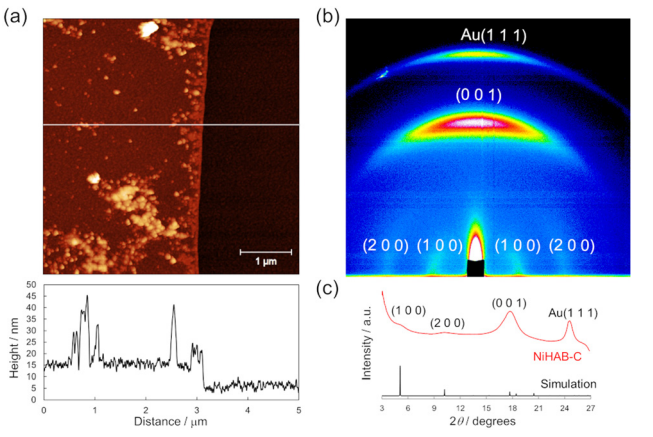

Fig. 4 (a) AFM topography image and height analysis at the corresponding white line of NiHAB-C. (b) Two-dimensional scattering image obtained by GIXS and (c) diffraction pattern converted from the scattering image of NiHAB-C.

solutions of concentrations 2.3 and 0.1 M, respectively (Table 1 and Fig. S3, ESI†). The OM images revealed a uniform grey film on NiHAB-F. Simultaneously, NiHAB-G still exhibited small black domains on its surface, thus indicating that the over-reaction of NiHAB was more effectively suppressed at high NH_3 concentrations and low metal ion and ligand concentrations (Fig. 5a and b). The AFM images showed that both samples had modified areas with thicknesses of 5 and 2 nm for NiHAB-F and NiHAB-G, respectively, thus corresponding to approximately 15 and 6 layers of NiHAB, respectively (Fig. 5c and d). Domains approximately twice the height of the modified area were also observed, implying the partial overgrowth of NiHAB. Furthermore, the root means square values of the modified region and gold surface for NiHAB-F were 1.1 and 1.0 nm, respectively, and 0.7 and 0.6 nm for NiHAB-G, thus indicating a uniform NiHAB formation on the electrodes while maintaining the surface roughness (Fig. S10, ESI†). The Raman spectra of NiHAB-F and NiHAB-G exhibited peaks derived from the NiHAB framework (Fig. 1a and Fig. S11a, ESI†). Furthermore, the XPS results exhibited the respective peaks of Ni $2p_{3/2}$, Ni $2p_{1/2}$, and N 1s with the calculated atomic ratios of Ni : N of 1 : 3.8 for NiHAB-F and 1 : 4.2 for NiHAB-G, thus corresponding to the expected ratio of the NiHAB structure (Ni : N = 1 : 4) (Fig. S11b and c, ESI†). These spectroscopic results confirmed the formation of the NiHAB structure. The 2D scattering image of NiHAB-F showed a scattering spot derived from the (0 0 1) plane of NiHAB in the out-of-plane direction (Fig. S12, ESI†). Although the scattering from the (1 0 0) plane of NiHAB was not clearly displayed because of the thinness of the sample and the overlap with a strong background signal from the incident X-rays, the face-on arrangement of NiHAB on the electrode was maintained when the synthesis was performed at low-concentrations.

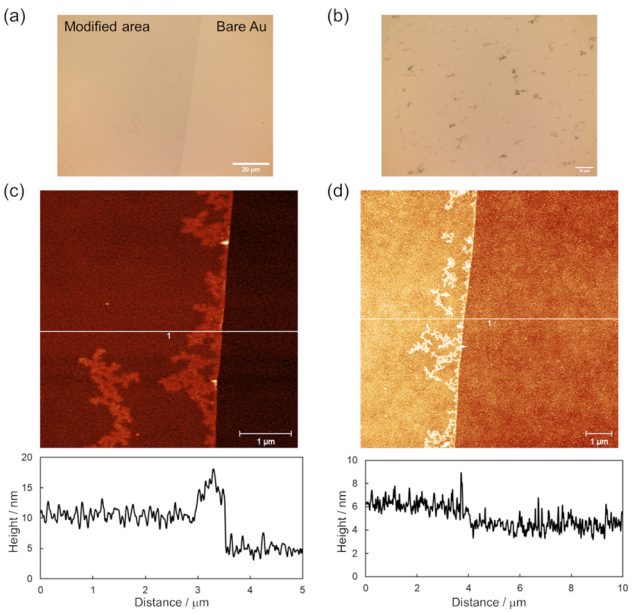

Fig. 5 OM of (a) NiHAB-F and (b) NiHAB-G, and AFM topography images and height profiles at the corresponding white lines of (c) NiHAB-F and (d) NiHAB-G.

The electrochemical synthesis of CoHAB and CuHAB under the optimised conditions was also investigated. CoHAB has been previously synthesized at 0.21 V *vs.* Ag/AgCl, and an application potential of −0.10 V *vs.* Ag/AgCl was chosen since the first oxidation peak of the electrolyte solution ended at this potential in the cyclic voltammogram (Fig. S13, ESI†). Although the Raman spectra of both CoHAB-A and CoHAB-B prepared on Au electrodes at 0.21 and −0.10 V *vs.* Ag/AgCl, respectively, were in accordance with those of a previous study,[16] they did not show any significant scattering patterns in the GIXS measurements, thus indicating their amorphous nature (Fig. S14, ESI†). A possible reason for the amorphous nature of CoHAB even in the synthesis at the lower oxidation potential is that Co^{2+} is a d^7 transition metal ion that can assume not only square planar but also other coordination geometries such as tetrahedral and octahedral, which prevents the formation of two-dimensional structures. Hence, it is more difficult for CoHAB to assume a high crystallinity than NiHAB.

The first oxidation peak of the reaction mixture of CuHAB ended at −0.20 V *vs.* Ag/AgCl (Fig. S15, ESI†) and the CuHAB prepared at the corresponding potential (CuHAB-B) showed a dark purple modified area and the GIXS measurements revealed an anisotropic scattering pattern suggesting a unit cell size for CuHAB (eclipsed stacking structure, *P*6/*mmm*, a = 13 Å, c = 3.2 Å) (Fig. S3 and S16, ESI†). Simultaneously, a rough surface morphology consisting of small grains of ∼60 nm in height was observed in the AFM measurements (Fig. S16, ESI†). Performing the synthesis in an electrolyte solution with copper ions and HAB concentrations diluted ten times resulted in the uniform formation of CuHAB-F (Fig. S17a, ESI†). The height analysis at the edge of CuHAB-F by AFM revealed a thickness of approximately 2 nm (Fig. S17b, ESI†). The Raman and XP spectra, in addition to the Cu and N atomic ratio value calculated from XPS (Cu : N = 1 : 4) and were in accordance with the previously reported data (Fig. S17c and d, ESI†).[23,27] Furthermore, the scattering pattern of CuHAB-F revealed the anisotropic formation of CuHAB on the Au electrode in a face-on orientation manner (Fig. S17e, ESI†).

The electrochemical activity of CoHAB-B and CuHAB-F were also investigated (Fig. S18, ESI†). CoHAB-B showed two broad oxidation peaks at *ca.* 0.47 V and 0.11 V *vs.* Fc^+/Fc and a broad reduction peak at −0.52 V *vs.* Fc^+/Fc, suggesting the slow redox reaction. The voltammogram of CuHAB-F exhibited several broad redox waves derived from a slow multistep redox reaction.

The MHAB (M = Ni, Cu) formation process in the face-on orientation manner on gold electrodes can be proposed as follows (Fig. 6a). Initially, metal ions and HAB ligands form flat bis(diamino)metal moieties in the electrolyte solution because Ni^{2+} and Cu^{2+} ion are d^8 and d^9 transition metal ions which have a preference to form square planar complexes, respectively. In this step, NH_3 is expected to work as a competitor of HAB decreasing the formation rate of bis(diamino)metal moieties, especially under the condition of high NH_3 concentration. Then, the formed complexes are adsorbed on a gold electrode in a flat orientation because of the interaction between the aromatic ring

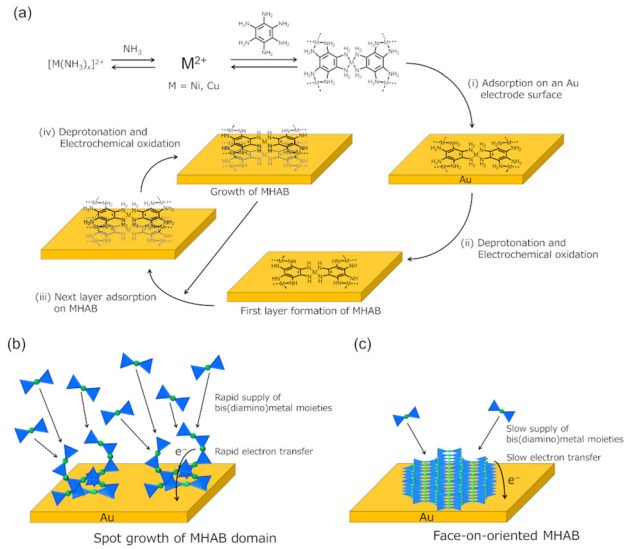

Fig. 6 (a) Proposed MHAB (M = Ni, Cu) formation mechanism in a face-on orientation manner. Schematic illustrates MHAB growth mechanisms at high oxidation potential and at high concentrations of building blocks (b) and at low oxidation potential and at low concentrations of building blocks (c).

and gold surface.[32–34] The adsorbed bis(diamino)metal moieties are converted to the bis(diimino)metal form by electrochemical oxidation and deprotonation by a base, thus giving the first layer of two-dimensional MHAB. Further adsorption of bis(diamino)metal moieties on the formed MHAB layer occurs because of π–π interactions and the electrochemical oxidation of the attached layer can progress by the through-space electron transfer *via* the overlapped π-conjugated orbitals between the stacked layers.[9] These adsorption and oxidation processes are repeated until the bis(diamino)metal moieties existing near the electrode surface are consumed, which can explain the thinner film formation observed at the low metal ion and HAB ligand concentrations. The applied potential affects the growth rate of MHAB. At a high oxidation potential, a large overpotential for the oxidation reaction of bis(diamino)metal moieties gives a large electron transfer rate. In this situation, the bis(diamino)metal moieties adsorbed on the electrode and the MHAB domains are immediately oxidized (Fig. 6b). Hence, the MHAB formation will proceed kinetically and rapidly at the highly reactive points such as the edges of Au domains rather than the flat planes of Au domains, giving the rough topographies observed in Fig. 2a and c. Furthermore, a rapid supply of bis(diamino)metal moieties to the electrode surface under the condition of a high concentration of building blocks also induces spot growth of MHAB. In contrast, a small electron transfer rate at a low oxidation potential and slow supply of bis(diamino)metal moieties under the condition of a low concentration of building blocks are preferred for a uniformed crystalline MHAB formation because the film growth is expected to be more thermodynamically controlled (Fig. 6c). As a result, under the optimal conditions (applying a low oxidation potential, high concentration of ammonia solution, and low concentration of building blocks), a slow MHAB growth results in a face-on orientation manner on the gold electrode.

Conclusions

This study reported a facile and rapid electrochemical oxidation method for the synthesis of MHAB (M = Ni, Cu) with face-on anisotropy and nanometre thickness on an electrode. The optimal reaction conditions were investigated and the results revealed that applying a low oxidation potential, high concentration of ammonia solution, and low concentration of building blocks were suitable for an oriented and uniform MHAB formation owing to the effective depression of local growth. Furthermore, a mechanism for the anisotropic growth of MHAB on the electrode was proposed. The results of this study can be applied to other CONASHs composed of π-conjugated ligands with amino ligating groups which can thus contribute to further unveiling the CONASH growth mechanism at liquid–solid interfaces. Furthermore, this simple anisotropic synthesis method proposed for the synthesis of crystalline CONASHs can contribute to the development of high-performance devices.

Conflicts of interest

There are no conflicts to declare.

Acknowledgements

This work was financially supported by JSPS KAKENHI (Grant Number: JP19H05460, 22K14569, and 22K05055) and the White Rock Foundation. Synchrotron radiation experiments were performed at BL05XU in SPring-8 (Hyogo, Japan). XPS measurements were supported by the Advanced Research Infrastructure for Materials and Nanotechnology in Japan (ARIM) of the Ministry of Education, Culture, Sports, Science and Technology (MEXT) (JPMXP12-A-22-UT-0007 & JPMXP12-A-23-UT-0025).

References

1 W. Wang, W. Zhao, H. Xu, S. Liu, W. Huang and Q. Zhao, *Coord. Chem. Rev.*, 2021, **429**, 213616.
2 Y.-L. Liu, X.-Y. Liu, L. Feng, L.-X. Shao, S.-J. Li, J. Tang, H. Cheng, Z. Chen, R. Huang, H.-C. Xu and J.-L. Zhuang, *ChemSusChem*, 2022, **15**, e202102603.
3 D. Rodríguez-San-Miguel, C. Montoro and F. Zamora, *Chem. Soc. Rev.*, 2020, **49**, 2291–2302.
4 H. Maeda, K. Takada, N. Fukui, S. Nagashima and H. Nishihara, *Coord. Chem. Rev.*, 2022, **470**, 214693.
5 B. Ding, M. B. Solomon, C. F. Leong and D. M. D'Alessandro, *Coord. Chem. Rev.*, 2021, **439**, 213891.
6 X. Mu, W. Wang, C. Sun, C. Wang and M. Knez, *Adv. Mater. Interfaces*, 2021, **8**, 2002151.
7 H. Zhong, M. Wang, G. Chen, R. Dong and X. Feng, *ACS Nano*, 2022, **16**, 1759–1780.
8 T. Yue, C. Xia, X. Liu, Z. Wang, K. Qi and B. Y. Xia, *ChemElectroChem*, 2021, **8**, 1021–1034.
9 L. S. Xie, G. Skorupskii and M. Dincă, *Chem. Rev.*, 2020, **120**, 8536–8580.

10 C. Park, J. W. Baek, E. Shin and I.-D. Kim, *ACS Nanosci. Au*, 2023, **3**, 353–374.
11 M. Hmadeh, Z. Lu, Z. Liu, F. Gándara, H. Furukawa, S. Wan, V. Augustyn, R. Chang, L. Liao, F. Zhou, E. Perre, V. Ozolins, K. Suenaga, X. Duan, B. Dunn, Y. Yamamoto, O. Terasaki and O. M. Yaghi, *Chem. Mater.*, 2012, **24**, 3511–3513.
12 R. W. Day, K. Bediako, M. Rezaee, L. R. Parent, G. Skorupskii, M. Q. Arguilla, C. H. Hendon, I. Stassen, N. C. Gianneschi, P. Kim and M. Dincă, *ACS Cent. Sci.*, 2019, **5**, 1959–1964.
13 J.-H. Dou, N. Q. Arguilla, Y. Luo, J. Li, W. Zhang, L. Sun, J. L. Mancuso, L. Yang, T. Chen, L. R. Parent, G. Skorupskii, N. J. Libretto, C. Sun, M. C. Yang, P. V. Dip, E. J. Brignole, J. T. Miller, J. Kong, C. H. Hendon, J. Sun and M. Dincă, *Nat. Mater.*, 2021, **20**, 222–228.
14 D.-G. Ha, M. Rezaee, Y. Han, S. A. Siddiqui, R. W. Day, L. S. Xie, B. J. Modtland, D. A. Muller, J. Kong, P. Kim, M. Dincă and M. A. Baldo, *ACS Cent. Sci.*, 2021, **7**, 104–109.
15 D. Xia, K. Sakaushi, A. Lyalin, K. Wada, S. Kumar, M. Amores, H. Maeda, S. Sasaki, T. Taketsugu and H. Nishihara, *Small*, 2022, **18**, 2202861.
16 K. Wada, H. Maeda, T. Tsuji, K. Sakaushi, S. Sasaki and H. Nishihara, *Inorg. Chem.*, 2020, **59**, 10604–10610.
17 J. Park, M. Lee, D. Feng, Z. Huang, A. C. Hinckley, A. Yakovenko, X. Zou, Y. Cui and Z. Bao, *J. Am. Chem. Soc.*, 2018, **140**, 10315–10323.
18 M. R. Lukatskaya, D. Feng, S.-M. Bak, J. W. F. To, X.-Q. Yang, Y. Cui, J. I. Feldblyum and Z. Bao, *ACS Nano*, 2020, **14**, 15919–15925.
19 S. C. Wechsler and F. Z. Amir, *ChemSusChem*, 2019, **13**, 1491–1495.
20 D. Feng, T. Lei, M. R. Lukatskaya, J. Park, Z. Huang, M. Lee, L. Shaw, S. Chen, A. A. Yakovenko, A. Kulkarni, J. Xiao, K. Fredrickson, J. B. Tok, X. Zou, Y. Cui and Z. Bao, *Nat. Energy*, 2018, **3**, 30–36.
21 I. Stassen, J.-H. Dou, C. Hendon and M. Dincă, *ACS Cent. Sci.*, 2019, **5**, 1425–1431.
22 C. Liu, Y. Gu, C. Liu, S. Liu, X. Li, J. Ma and M. Ding, *ACS Sens.*, 2021, **6**, 429–438.
23 K.-H. Wu, J. Cao, T. Pal, H. Yang and H. Nishihara, *Appl. Energy Mater.*, 2021, **4**, 5403–5407.
24 C. Li, L. Shi, L. Zhang, P. Chen, J. Zhu, X. Wang and Y. Fu, *J. Mater. Chem. A*, 2020, **8**, 369–379.
25 J. Park, Z. Chen, R. A. Flores, G. Wallnerström, A. Kulkarni, J. K. Nørskov, T. F. Jaramillo and Z. Bao, *ACS Appl. Mater. Interfaces*, 2020, **12**, 39074–39081.
26 E. J. H. Phua, K.-H. Wu, K. Wada, T. Kusamoto, H. Maeda, J. Cao, R. Sakamoto, H. Masunaga, S. Sasaki, J.-W. Mei, W. Jiang, F. Liu and H. Nishihara, *Chem. Lett.*, 2018, **47**, 126–129.
27 H. Maeda, K. Takada, N. Fukui, J. Ukai, N. Honma, S. Sasaki, H. Masunaga, K. Kato and H. Nishihara, *J. Inorg. Organomet. Polym. Mater.*, 2023, DOI: **10.1007/s10904-023-02920-5**.
28 Q. Zhang, H. Dong and W. Hu, *J. Mater. Chem. C*, 2018, **6**, 10672–10686.
29 N. Manjunatha, M. Imadadulla, K. S. Lokesh and K. R. V. Reddy, *Dyes Pigm.*, 2018, **153**, 213–224.
30 K.-H. Wu, R. Sakamoto, H. Maeda, E. J. H. Phua and H. Nishihara, *Molecules*, 2021, **26**, 4267.
31 J. Park, A. C. Hinckley, Z. Huang, D. Feng, A. A. Yakovenko, M. Lee, S. Chen, X. Zou and Z. Bao, *J. Am. Chem. Soc.*, 2018, **140**, 14533–14537.
32 H. Dahms and M. Green, *J. Electrochem. Soc.*, 1963, **110**, 1075.
33 P. Gao and M. J. Weaver, *J. Phys. Chem.*, 1985, **89**, 5040–5046.
34 X. Gao, J. P. Davies and M. J. Weaver, *J. Phys. Chem.*, 1990, **94**, 6858–6864.